ISSN 1674-1056
http://cpb.iphy.ac.cn
http://iopscience.iop.org/cpb
中国物理 B
Chinese Physics
中国物理
Chinese Physics B

Mott transition in ruby lattice Hubbard model

An Bao(保安)

Citation: Chin. Phys. B . 2019, 28(5): 057101. **doi:** 10.1088/1674-1056/28/5/057101
Journal homepage: http://cpb.iphy.ac.cn; http://iopscience.iop.org/cpb

What follows is a list of articles you may be interested in

Review of gallium oxide based field-effect transistors and Schottky barrier diodes

Zeng Liu(刘增), Pei-Gang Li(李培刚), Yu-Song Zhi(支钰崧), Xiao-Long Wang(王小龙), Xu-Long Chu(褚旭龙), Wei-Hua Tang(唐为华)\

Chin. Phys. B . 2019, 28(1): 017105. **doi:** 10.1088/1674-1056/28/1/017105

Metal-to-insulator transition in two-dimensional ferromagnetic monolayer induced by substrate

Can Qi(齐灿), Jun Hu(胡军)

Chin. Phys. B . 2018, 27(7): 077106. **doi:** 10.1088/1674-1056/27/7/077106

Doping-driven orbital-selective Mott transition in multi-band Hubbard models with crystal field splitting

Yilin Wang(王义林), Li Huang(黄理), Liang Du(杜亮), Xi Dai(戴希)

Chin. Phys. B . 2016, 25(3): 037103. **doi:** 10.1088/1674-1056/25/3/037103

Phase diagram of the Fermi–Hubbard model with spin-dependent external potentials: A DMRG study

Wei Xing-Bo, Meng Ye-Ming, Wu Zhe-Ming, Gao Xian-Long

Chin. Phys. B . 2015, 24(11): 117101. **doi:** 10.1088/1674-1056/24/11/117101

Disappearance of the Dirac cone in silicene due to the presence of an electric field

D. A. Rowlands, Zhang Yu-Zhong

Chin. Phys. B . 2014, 23(3): 037101. **doi:** 10.1088/1674-1056/23/3/037101

Mott transition in ruby lattice Hubbard model*

An Bao(保安)†

Beijing National Laboratory for Condensed Matter Physics, Institute of Physics, Chinese Academy of Sciences, Beijing 100190, *China*

(Received 26 September 2018; revised manuscript received 27 February 2019; published online 4 April 2019)

Mott transition in a ruby lattice with fermions described by the Hubbard model including on-site repulsive interaction is investigated by combining the cellular dynamical mean-field theory and the continuous-time quantum Monte Carlo algorithm. The effect of temperature and on-site repulsive interaction on the metallic–insulating phase transition in ruby lattice with fermions is discussed based on the density of states and double occupancy. In addition, the magnetic property of each phase is discussed by defining certain magnetic order parameters. Our results show that the antiferromagnetic metal is found at the low temperature and weak interaction region and the antiferromagnetic insulating phase is found at the low temperature and strong interaction region. The paramagnetic metal appears in whole on-site repulsive interaction region when the temperature is higher than a certain value and the paramagnetic insulator appears at the middle scale of temperature and on-site repulsive interaction.

Keywords: Mott transition, ruby lattice, Hubbard model, cellular dynamical mean-field theory

PACS: 71.30.+h, 71.27.+a, 71.10.Fd **DOI:** 10.1088/1674-1056/28/5/057101

1. Introduction

A honeycomb lattice and its analogs has attracted considerable great interest in condensed matter physics for many years due to their significant role in theoretical research and promising potential in application. Many intriguing quantum phases, have been observed in these systems, such as topological insulators, Bose–Einstein condensation, and the quantum Hall effect.[1–17] Among the variety of two-dimensional lattices, the ruby lattice may be found in an entirely new class of stacked two-dimensional topological insulators $Bi_{14}Rh_3I_9$, which is the most interesting one.[18] As shown in Fig. 1, the crystal structure of $Bi_{14}Rh_3I_9$ exhibits a periodic alternating stacking of two-dimensional bismuth-rhodium networks and insulating spacers, where the two-dimensional bismuth-rhodium networks can be understood as a decorated honeycomb lattice, or ruby lattice. A ruby lattice with fermions may also be simulated by an optical lattice with cold atoms, in which the interaction between the trapped atoms can be tuned by the Feshbach resonance.

The representative work on ruby lattice includes: the investigation of the dispersion of the topologically protected spin-filtered edge states of the quantum spin Hall state on ruby nets with zigzag and armchair edges; the finding of fractional quantum Hall effect in ruby lattice with Rashba spin–orbit coupling under the framework of a tight-binding model; and the realization of a Chern insulator with an extremely flat lowest band in a ruby lattice, through considering the simplified spin-polarized version of tight-binding model with spin–orbit coupling.[19,20] In addition, some other intriguing results have also been obtained by using the two-dimensional Ising model and the Kitaev spin model on ruby lattice.[21–23] However, few have considered the effect of the on-site repulsive interaction on the Mott transition in ruby lattice with fermions, which plays a vital role on the quantum phase transition of strongly correlated systems.

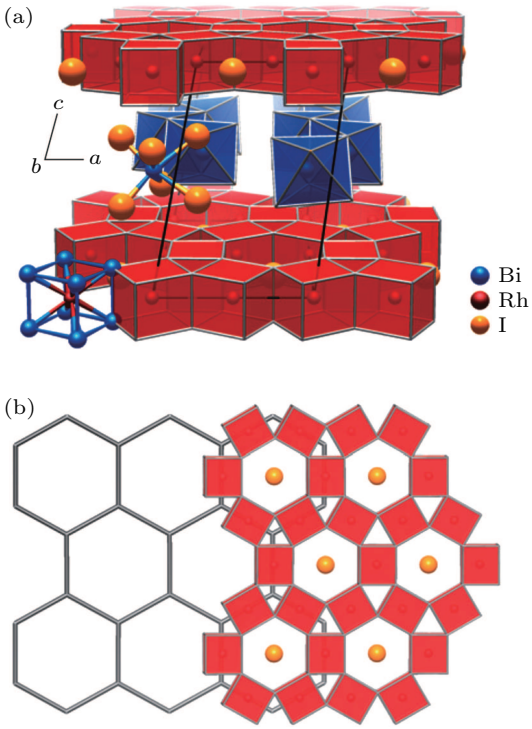


Fig. 1. (a) The sketch map of $Bi_{14}Rh_3I_9$ lattice structure and the prototype of ruby lattice in this material at the certain plane. The blue sites, red sites, and yellow ones represent bismuth, rhodium, and iodine, respectively. (b) Aerial view of $Bi_{14}Rh_3I_9$ reproduced from Ref. [18].

In this work, the celebrated Hubbard model[24–27] with

*Project supported by Inner Mongolia Natural Science Foundation, China (Grant No. 06021601).

†Corresponding author. E-mail: baoan204@aliyun.com

© 2019 Chinese Physical Society and IOP Publishing Ltd

the on-site repulsive interaction is adopted to describe fermions in a ruby lattice. The cellular dynamical mean-field theory (CDMFT)[28–32] is used to map the lattice to a self-consistent embedded cluster in real space and the continuous-time quantum Monte Carlo (CTQMC)[33,34] algorithm is used as an impurity solver to deal with the mean field equations. The CDMFT has proven to be more successful than the dynamical mean field theory[35,36] and the CTQMC is more accurate than the general quantum Monte Carlo method. The density of states and the double occupancy that play critical roles in the decision of Mott metal–insulator transition have been calculated based on the single-particle's Green function, as obtained by the CDMFT and CTQMC. The phase diagrams reflect the effect of temperature and on-site repulsive interaction on phase transition and they show the magnetic property of each phase of the ruby lattice with fermions.

2. Model and methods

2.1. Model

As shown in Fig. 2(a), the ruby lattice can be viewed as an expanded honeycomb lattice with triangles replacing the vertices and squares replacing the bonds. The Hamiltonian of the single-band Hubbard model with on-site repulsive interaction used to describe fermions in ruby lattice can be written as follows:

$$H = -t_1 \sum_{\langle i,j\rangle,\sigma} (c^{\dagger}_{i\sigma} c_{j\sigma} + c^{\dagger}_{j\sigma} c_{i\sigma}) - t_2 \sum_{\langle\langle i,j\rangle\rangle,\sigma} (c^{\dagger}_{i\sigma} c_{j\sigma} + c^{\dagger}_{j\sigma} c_{i\sigma}) + U \sum_i n_{i\uparrow} n_{i\downarrow}, \quad (1)$$

where the operator $c^{\dagger}_{i\sigma}$ creates a particle with spin σ on site i and the operator $c_{j\sigma}$ annihilates a particle with spin σ on site j. t_1 is the hopping amplitude between the nearest two sites in the same triangle while t_2 represents the hopping amplitude between the nearest two sites belonging to two different triangles. $n_{i\sigma} = c^{\dagger}_{i\sigma} c_{i\sigma}$ is the density operator and U is the on-site repulsive interaction. $\langle i, j\rangle$ implies the nearest two sites in the same triangle and $\langle\langle i, j\rangle\rangle$ indicates the nearest two sites belonging to two different triangles.

For $U = 0$, the Hubbard model converts to the tight binding model and the Hamiltonian in momentum space becomes $H_0 = \sum_k \Psi^{\dagger}_k \mathcal{H}^0_k \Psi_k$, where $\Psi_k = (c_{Ak\uparrow}, c_{Bk\uparrow}, c_{Ck\uparrow}, c_{Dk\uparrow}, c_{Ek\uparrow}, c_{Fk\uparrow}, c_{Ak\downarrow}, c_{Bk\downarrow}, c_{Ck\downarrow}, c_{Dk\downarrow}, c_{Ek\downarrow}, c_{Fk\downarrow})^{\mathrm{T}}$. The index $i = $ A, B, C, D, E, F of the creation and annihilation operators represents the six sites in each unit cell, as illustrated in Fig. 2(a), k is the location in the first Brillouin zone, and $\uparrow$ and $\downarrow$ indicate the spin-up and spin-down states, respectively. Since H_0 is decoupled in the spin states, so $\mathcal{H}^0_k$ is block diagonalized (i.e., two blocks representing spin-up and spin-down electrons are the same) and is expressed as follows:

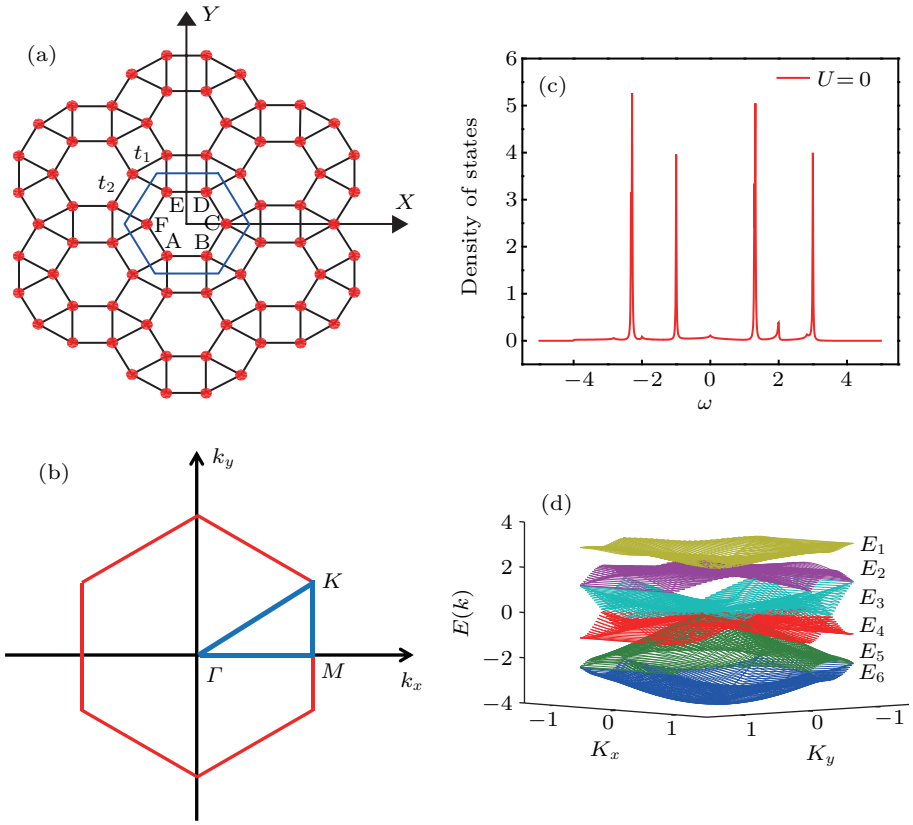


Fig. 2. Basic information of ruby lattice. (a) The sketch map of the ruby lattice. (b) The first Brillouin zone of the ruby lattice. (c) The density of states of the isotropic ($\lambda = 1$) ruby lattice which is half-filled with fermions without interaction at $T = 0.2$. (d) The energy dispersion in the first Brillouin zone of the ruby lattice.

$$\mathcal{H}_k^0 = -\begin{pmatrix} 1 & 0 \\ 0 & 1 \end{pmatrix} \otimes \begin{pmatrix} 0 & t_1 & t_2 e^{-i(ak_x+bk_y)/2} & 0 & t_2 e^{-i2bk_y} & t_1 \\ t_1 & 0 & t_1 & t_2 e^{-i2bk_y} & 0 & t_2 e^{i(ak_x-bk_y)/2} \\ t_2 e^{i(ak_x+bk_y)/2} & t_1 & 0 & t_1 & t_2 e^{i(ak_x-bk_y)/2} & 0 \\ 0 & t_2 e^{ibk_y} & t_1 & 0 & t_1 & t_2 e^{i(ak_x+bk_y)/2} \\ t_2 e^{ibk_y} & 0 & t_2 e^{-i(ak_x-bk_y)/2} & t_1 & 0 & t_1 \\ t_1 & t_2 e^{-i(ak_x-bk_y)/2} & 0 & t_2 e^{-i(ak_x+bk_y)/2} & t_1 & 0 \end{pmatrix}, \quad (2)$$

where $a = (3+\sqrt{3})/2$ and $b = (1+\sqrt{3})/2$ are parameters which are related to the lattice constant.

The energy dispersions of isotropic ($\lambda = t_1/t_2 = 1$) and anisotropic ($\lambda = t_1/t_2 \neq 1$) ruby lattices with fermions are presented in Fig. 3. It can be seen from Fig. 3(a) that the ruby lattice which is one third filled with fermions is in an insulating state for $\lambda = 0.5$. For the isotropic case, the system is in a metallic state where the bands E_3 and E_4 degenerate along the line between Γ point and M point. The system is transferred to the insulating state when the ruby lattice is half-filled with fermions for $\lambda = 2.0$ and one-sixth-filled with fermions for $\lambda = 10$.

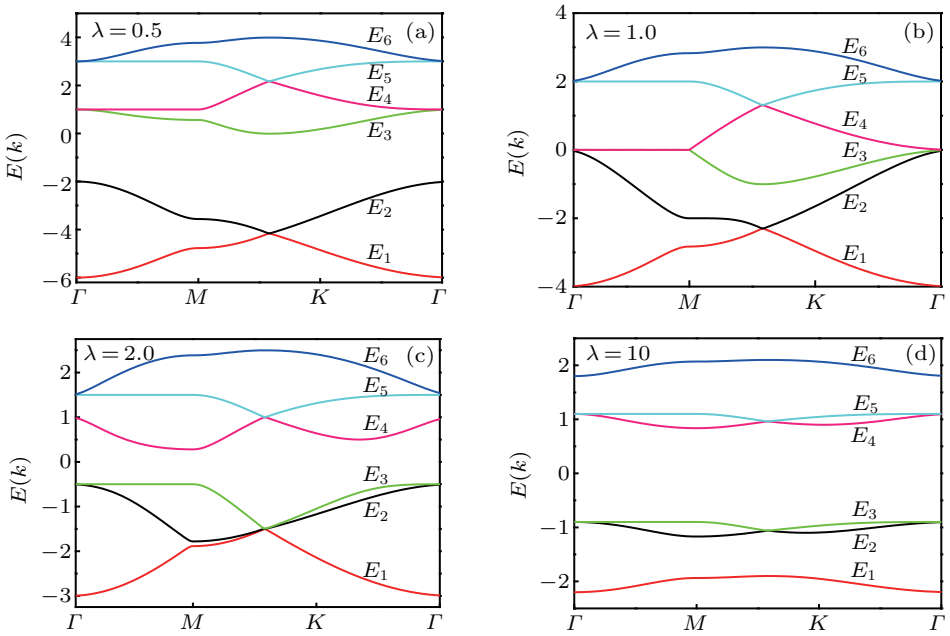


Fig. 3. Energy band of the ruby lattice in the first Brillouin zone. (a) The energy dispersion of the anisotropic ruby lattice ($\lambda = t_1/t_2$, $\lambda = 0.5$). (b) The energy dispersion of the isotropic ruby lattice while $\lambda = 1.0$ (c) and (d) The energy dispersions of the anisotropic ruby lattice for $\lambda = 2.0$ and $\lambda = 10$, respectively. $t_1 = 1$ for all cases.

2.2. Methods

2.2.1. Cellular dynamical mean-field theory

As an extension of the dynamical mean-field theory, the cellular dynamical mean-field theory, which has been proven to be quite efficient in describing the low dimensional strongly correlated systems with strong quantum fluctuation, is used to map the ruby lattice onto a six-site effective cluster embedded in a self-consistent bath field. The self-consistent calculations start with a guessed tiny self-energy $\Sigma(i\omega)$ which is independent of momentum.[37] The Weiss field $g(i\omega)$ is given by the coarse-grained Dyson equation

$$g^{-1}(i\omega) = \left[\sum_k \frac{1}{i\omega + \mu + t(k) - \Sigma(i\omega)}\right]^{-1} + \Sigma(i\omega), \quad (3)$$

where ω is the Matsubara frequency, μ is the chemical potential, and $\sum_k$ implies the sum over all wave vectors in the reduced Brillouin zone of the superlattice. $t(k)$ is the Fourier transform of the hopping amplitude of the Hamiltonian in Eq. (1) and mathematically equals to the second factor of the direct product in Eq. (2), which is a six-dimensional matrix for the ruby lattice under the framework of cellular dynamical mean field theory. The cluster Green function $G(i\omega)$ is obtained by continuous-time quantum Monte–Carlo algorithm as the impurity solver and 1×10^6 continuous-time quantum Monte–Carlo sweeps are carried out for each CDMFT loop. New self-energy $\Sigma(i\omega)$ is obtained by Dyson equation $\Sigma(i\omega) = g^{-1}(i\omega) - G^{-1}(i\omega)$.

2.2.2. Continuous-time quantum Monte Carlo algorithm

The continuous-time quantum Monte Carlo algorithm starts the procedure from a series expansion of the partition function in the powers of interaction

$$Z = \mathrm{Tr}\, e^{-\beta H} = Z_0 T_\tau \left[\sum_k \frac{1}{k}\left(-\int_0^\beta H_1(\tau)\, d\tau\right)^k\right], \quad (4)$$

where $Z_0 = \mathrm{Tr}\, \mathrm{e}^{-\beta H_0}$ is the unperturbed partition function, T_τ is the time-ordering operator, and $H_1(\tau) = \mathrm{e}^{\tau H_0} H_1 \mathrm{e}^{-\tau H_0}$ is the mapping of H_1 in interaction picture. By inserting $H_1 = U\sum_i n_{i\uparrow} n_{i\downarrow}$ into Eq. (4), we obtain

$$Z = Z_0 \sum_k \frac{-U^k}{k!} \int \cdots \int \mathrm{d}r_1 \cdots \mathrm{d}r_2 \langle T_\tau n_\uparrow(r_1) \cdots n_\uparrow(r_k)\rangle \times \langle T_\tau n_\downarrow(r_1) \cdots n_\downarrow(r_k)\rangle.$$

Based on Wick's theorem, the time-ordering operator $\langle T_\tau n_\sigma(r_1) \cdots n_\sigma(r_k)\rangle$ for each order of k can be expressed by the determinants of matrix

$$\mathcal{D}(k) = \begin{pmatrix} G^0(r_1,r_1) & G^0(r_1,r_2) & \dots & G^0(r_1,r_k) \\ G^0(r_2,r_1) & G^0(r_2,r_2) & \dots & G^0(r_2,r_k) \\ \vdots & \vdots & \vdots & \vdots \\ G^0(r_k,r_1) & G^0(r_k,r_2) & \dots & G^0(r_k,r_k) \end{pmatrix}, \quad (5)$$

which consists of the non-interacting Green functions G^0. There is no spin index in $D(k)$ for the determinants due to the equivalence of spin-un and spin-down. Through integrand of Eq. (5), we can obtain the weight of order k

$$W_k = (-\delta\tau U)^k \det D_\uparrow(k) \det D_\downarrow(k), \quad (6)$$

where $\delta\tau = \beta/L$ is the slice of imaginary time. We can obtain the standard Metropolis acceptance ratio R of adding vertex by the detailed balance condition

$$\frac{1}{LN} W_k P_{k\to k+1} = \frac{1}{k+1} W_{k+1} P_{k+1\to k}, \quad (7)$$

$$R = \frac{P_{k\to k+1}}{P_{k+1\to k}} = -\frac{U\beta N}{k+1} \left(\frac{\det D_\uparrow(k+1) \det D_\downarrow(k+1)}{\det D_\uparrow(k) \det D_\downarrow(k)} \right). \quad (8)$$

Here $P_{k\to k+1}$ is the probability to increase the order from k to k+1 ($P_{k+1\to k}$ is the probability to decrease the order from k+1 to k), $1/(LN)$ is the probability to choose a position in time and space for the vertex you intend to add, while $1/(k+1)$ is the probability to choose one vertex you intend to remove from the existing $k+1$ ones. To calculate the ratio R, we have to deal with the function $\lambda = \det D(k+1)/\det D(k) = \det(I + (d(k+1) - D(k))M(k))$, in which

$$M(k+1) = \begin{pmatrix} \cdot & \cdot & \cdot & -L_{1,k+1}\lambda^{-1} \\ \cdot & M'_{i,j} & \cdot & -L_{2,k+1}\lambda^{-1} \\ \vdots & \vdots & \vdots & \vdots \\ \cdot & \cdot & \cdot & -L_{k,k+1}\lambda^{-1} \\ -\lambda^{-1}R_{k+1,1} & -\lambda^{-1}R_{k+1,2} & \dots & -\lambda^{-1} \end{pmatrix}, \quad (9)$$

$$M'_{i,j} = M(k)_{i,j} + L_{i,k+1}\lambda^{-1}R_{k+1,j}, \quad R_{i,j} = G^0(i,j)M(k)_{i,j},$$

$$L_{i,j} = M(k)_{i,l} G^0(l,j),$$

$$\det \begin{pmatrix} 1 & 0 & \dots & 0 & G^0(r_1,r_{k+1}) \\ 0 & 1 & \dots & 0 & G^0(r_2,r_{k+1}) \\ \vdots & \vdots & \vdots & \vdots & \vdots \\ 0 & 0 & \dots & 1 & G^0(r_k,r_{k+1}) \\ G^0(r_k,r_1) & G^0(r_k,r_2) & \dots & G^0(r_k,r_k) & G^0(r_{k+1},r_{k+1}) \end{pmatrix} = G^0(r_{k+1},r_{k+1}) - G^0(r_{k+1},r_i) M(k)_{i,j} G^0(r_j,r_{k+1}). \quad (10)$$

For the step $k-1$, we obtain the ratio R and update formulas of $M(k-1)$

$$R = \frac{k}{U\beta N} \left(\frac{\det D_\uparrow(k-1) \det D_\downarrow(k-1)}{\det D_\uparrow(k) \det D_\downarrow(k)} \right). \quad (11)$$

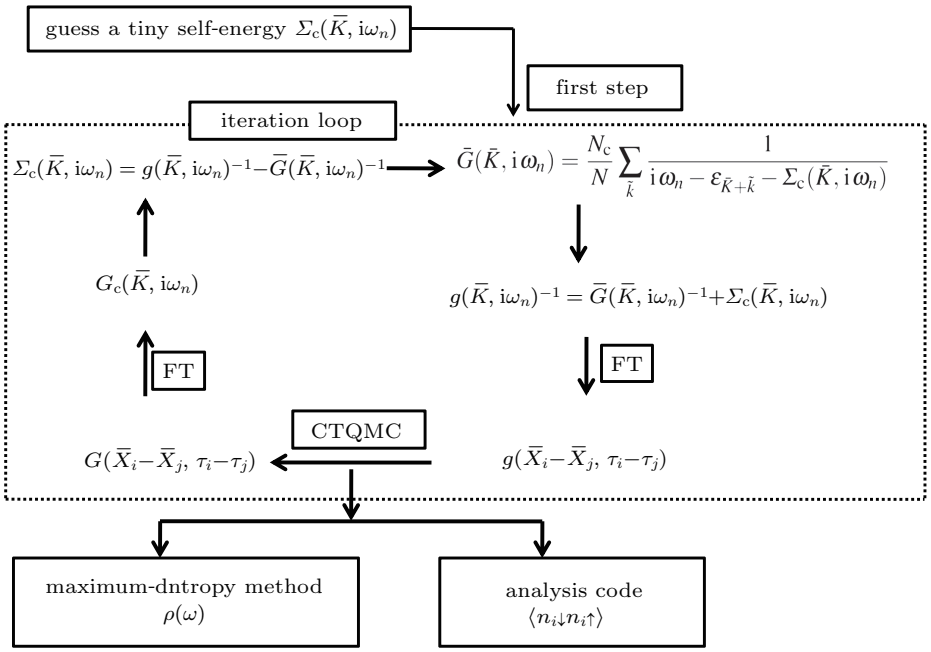


Fig. 4. The process of the self-consistent calculation for the ruby lattice. Iteration loop of the self-consistent calculation based on the CDMFT and the CTQMC are presented in detail. The self-consistent calculations start with a guessed tiny self-energy $\Sigma(i\omega)$. Weiss field $g(i\omega)$ is given by the coarse-grained Dyson equation and the cluster Green function $G(i\omega)$ is obtained by continuous-time quantum Monte-Carlo algorithm.

Using the updated formula for M, Green's function can be obtained both in imaginary time and at Matsubara frequencies

$$G(\tau-\tau') = G^0(\tau-\tau') - G^0(\tau-\tau_i)M_{i,j}G^0(\tau_j-\tau'), \quad (12)$$

$$G(\mathrm{i}\omega) = G_0(\mathrm{i}\omega) - G_0(\mathrm{i}\omega)\left[\frac{1}{\beta}\sum_{i,j}M_{i,j}\mathrm{e}^{-\omega(\tau_i-\tau_j)}\right]G_0(\mathrm{i}\omega). \quad (13)$$

This self-consistent iteration is carried out until the accuracy of the self-energy reaches what we expected. The detail of continuous time quantum Monte–Carlo algorithm could be found in the references.

3. Results

The density of states and the double occupancy are important quantities for the decision of metal–insulator phase transition in the two-dimensional strongly correlated systems. The density of states is given by $D(\omega) = -\frac{1}{\pi}\sum_{i=1}^{6}(\mathrm{Im}G_{ii}(\omega-\mathrm{i}\delta))$ (i is the lattice points' index in the cluster) and calculated by the maximum entropy method.[38] The six-fold rotation symmetry of the ruby lattice guarantees that the six sites' local densities of states are the same. Here, we present the density of states of isotropic ($\lambda = 1.0$) and anisotropic ($\lambda = 2.0$) ruby lattices with fermions. Figure 5(a) shows that the density of states of the isotropic ruby lattice at Matsubara frequency $\omega = 0$ decreases with the increase of the on-site repulsive interaction and opens a pseudogap around $U = 8.5$ for $T = 0.2$. The pseudogap indicates the Mott transition from metal state to insulating phase. For $U = 8$, the temperature for the metal–insulator transition is around $T = 0.13$ in the isotropic ruby lattice which can be seen in Fig. 5(b). Through combining Figs. 3(c) and 5(c), it can be conclude that the anisotropic ($\lambda = 2.0$) ruby lattice with fermions undergoes a transition from band insulator to Mott insulator around $U = 6$ and $T = 0.2$. Figure 5(d) shows that there is no pseudogap state but is precursor of Kondo resonance in the isotropic ($\lambda = 1.0$) ruby lattice at lower temperature $T = 0.1$ and small interaction regime, the phase corresponds to a Kondo metal. Strictly speaking, the transition at finite temperature decided by the opened pseudogap at $\omega = 0$ in density of states is actually a crossover.

The confinement of fermions in the lattice site of the ruby lattice with fermions can be described by double occupancy (D_{occ}) which is defined as $D_{\mathrm{occ}} = \partial F/\partial U = \frac{1}{6}\sum_i\langle n_{i\uparrow}n_{i\downarrow}\rangle$, where F is the free energy.[39,40] D_{occ} increases as the temperature decreases in the lower interaction regime and is almost independent of temperature in the large interaction region. The increase of D_{occ} at low temperatures means the suppression of the local moments due to the formation of quasiparticles. The independence of D_{occ} on interaction indicates that the itinerancy of the particles is suppressed by the large enough interaction ($U > U_{\mathrm{c}}$). D_{occ} can be used to check the phase-transition order because it is directly connected to the free energy. At finite temperature, the continuity of double occupancy as a function of interaction indicates crossover and the discontinuity accompanied by hysteresis is thought as a signal of first-order phase transition.[9] The smooth decrease of D_{occ} indicates that this phase transition is a second-order phase transition.

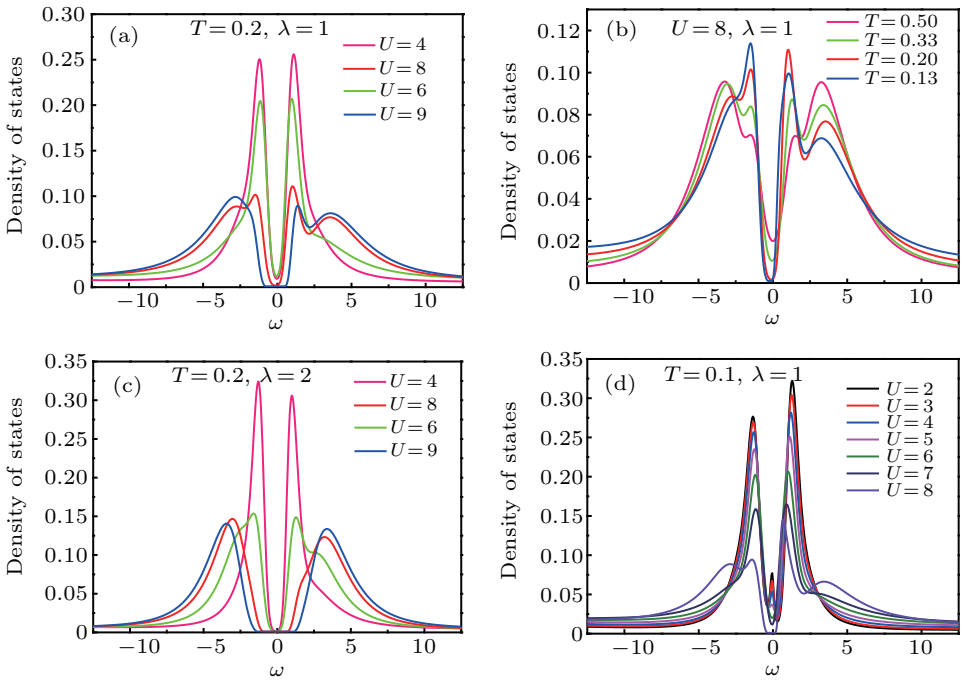


Fig. 5. (a) Density of states of isotropic ruby lattice for different interaction at $T = 0.2$. (b) Density of states of isotropic ruby lattice for different temperature at $U = 8$. (c) Density of states of anisotropic ruby lattice ($\lambda = 2.0$) for different interaction at $T = 0.2$. (d) Density of states of isotropic ruby lattice ($\lambda = 1.0$) at lower temperature ($T = 0.1$) for different interactions.

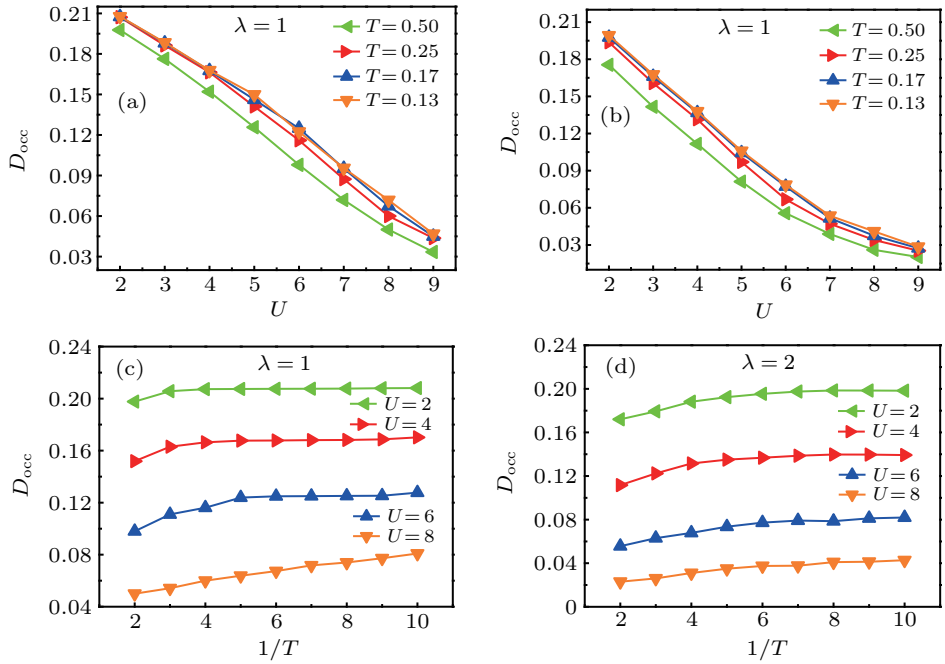


Fig. 6. (a) and (b) The double occupancy $D_{\rm occ}$ of isotropic and anisotropic ($\lambda = 2.0$) ruby lattices as a function of the interaction U for different temperature, respectively. (c) and (d) The double occupancy $D_{\rm occ}$ of isotropic and anisotropic ($\lambda = 2.0$) ruby lattices as a function of temperature T for different interactions, respectively.

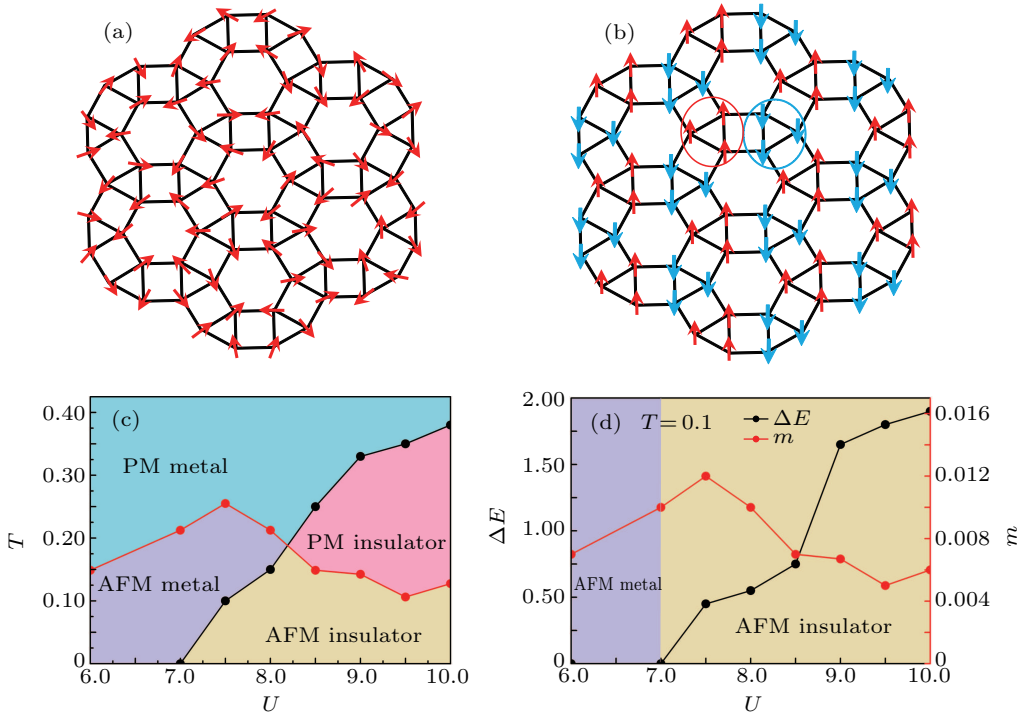


Fig. 7. Phase diagrams of the isotropic ruby lattice. (a) and (b) The sketch map of paramagnetic order and antiferromagnetic order in ruby lattice, respectively. (c) Competition between temperature and interaction for Mott transition in isotropic ruby lattice. (d) Relation between interaction and single particle gap ΔE, transition between antiferromagnetic metal and antiferromagnetic insulator in ruby lattice at $T = 0.1$.

When compared to the square lattice and honeycomb lattice, the ruby lattice is more complicated because of its substantial magnetic frustration. Therefore, it is a huge challenge to systematically discuss the magnetic property of such a substantially frustrated system. Here, we discuss the paramagnetic (PM) and antiferromagnetic (AFM) properties of metallic and insulating states of the ruby lattice with fermions through defining the magnetic order parameter $m = \frac{1}{N_c}\sum_i \text{sign}(i)(\langle n_{i\uparrow}\rangle - \langle n_{i\downarrow}\rangle)$, where $n_{i\sigma}$ is the particle density operator, $\text{sign}(i) = 1$ for $i =$ A, C, E and $\text{sign}(i) = -1$ if $i =$ B, D, F as shown in Fig. 2(a). From the definition of the magnetic order parameter, it can be known that $m = 0$ corresponds to the paramagnetic phase while $m \neq 0$ represents the antiferromagnetic phase. The sketch maps of paramagnetic and anti-

ferromagnetic orders are, respectively, shown in Figs. 7(a) and 7(b). For such a frustrated system, the pattern of magnetic order shown in Fig. 7(b) can only be stable in the regime $t_1 \gg t_2$ used to express the total magnetic order result of the isotropic ruby lattice instead of the exact spin direction on every single site. Figure 7(c) gives the phase diagram with the competition between interaction and temperature of ruby lattice with fermions while figure 7(d) shows the evolution of single particle gap (ΔE) and magnetic order parameter (m) as a function of interaction (U) when $\lambda = 1$ and $T = 0.1$.

4. Conclusion

A combination of cellular dynamical mean-field theory and continuous-time quantum Monte Carlo method was used to solve the Hubbard model on ruby lattice with fermions. The Mott transition in ruby lattice with fermions was discussed based on the density of states and the double occupancy. Meanwhile, the certain magnetic property of each phase in ruby lattice with fermions was presented by defining the specific magnetic order parameters. It can be seen clearly that both the antiferromagnetic and the paramagnetic states are found in the metallic phase and insulating phase at certain temperature regions and interaction scales. The antiferromagnetic metal and the antiferromagnetic insulator were, respectively, found in weak and strong on-site repulsive interaction regions at low temperatures. The paramagnetic metal appeared in whole on-site repulsive interaction scale above a certain temperature while the paramagnetic insulator appeared at the middle scale of temperature and on-site repulsive interaction. We hope that our study will be a useful step for understanding the interaction driven metal–insulator transition and will also provide practical instruction for the investigation on real materials, such as topological insulators.

References

[1] Martelo L Z, Dzierzawa M, Siffert L and Baeriswyl D 1997 *Z. Phys. B* **103** 335
[2] Yoshioka T, Koga A and Kawakami N 2009 *Phys. Rev. Lett.* **103** 036401
[3] Bao A, Tao H S, Liu H D, Zhang X Z and Liu W M 2014 *Sci. Rep.* **4** 6918
[4] Singh Y and Gegenwart P 2010 *Phys. Rev. B* **82** 064412
[5] Liu H D, Chen Y H, Lin H F, Tao H S and Liu W M 2014 *Sci. Rep.* **4** 4829
[6] Sorella S and Tosatti E 1992 *Europhys. Lett.* **19** 699
[7] Wu W, Chen Y H, Tao H S, Tong N H and Liu W M 2010 *Phys. Rev. B* **82** 245102
[8] Chen Y H, Tao H S, Yao D X and Liu W M 2012 *Phys. Rev. Lett.* **108** 246402
[9] Ohashi T, Kawakami N and Tsunetsugu H 2006 *Phys. Rev. Lett.* **97** 066401
[10] Bao A, Zhang X F and Zhang X Z 2015 *Chin. Phys. B* **24** 050310
[11] Raghu S, Qi X L, Honerkamp C and Zhang S C 2008 *Phys. Rev. Lett.* **100** 156401
[12] Rüegg A, Wen J and Fiete G A 2010 *Phys. Rev. B* **81** 205115
[13] Guo H M and Franz M 2009 *Phys. Rev. B* **80** 113102
[14] Shimizu Y, Miyagawa K, Kanoda K, Maesato M and Saito G 2003 *Phys. Rev. Lett.* **91** 107001
[15] Liu G C, Zhang P, Wang Z G and Li S S 2009 *Phys. Rev. B* **79** 035323
[16] Zhang M C, Hung H H, Zhang C W and Wu C J 2011 *Phys. Rev. A* **83** 023615
[17] Itou T, Oyamada A, Maegawa S, Tamura M and Kato R 2008 *Phys. Rev. B* **77** 104413
[18] Rasche B, Isaeva A, Ruck M, Borisenko S, Zabolotnyy V, Büchner B, Koepernik K, Ortix C, Richter M and Brink J van den 2013 *Nat. Mat.* **12** 422
[19] Hu X, Kargarian M and Fiete G A 2011 *Phys. Rev. B* **84** 155116
[20] Hou J M and Wang G X 2013 *Commun. Theor. Phys.* **60** 129
[21] Whitsitt S, Chua V and Fiete G A 2012 *New J. Phys.* **14** 115029
[22] Lin K Y and Ma W J 1983 *J. Phys. A: Math. Gen.* **16** 3895
[23] Kargarian M, Bombin H and Martin-Delgado M A 2010 *New J. Phys.* **12** 025018
[24] Hubbard J 1963 *Proc. R. Soc. Lond. A* **276** 238
[25] Gutzwiller M C 1963 *Phys. Rev. Lett.* **10** 159
[26] Aryanpour K, Pickett W E and Scalettar R T 2006 *Phys. Rev. B* **74** 085117
[27] Ohashi T, Momoi T, Tsunetsugu H and Kawakami N 2008 *Phys. Rev. Lett.* **100** 076402
[28] Kotliar G, Savrasov S Y, Pálsson G and Biroli G 2001 *Phys. Rev. Lett.* **87** 186401
[29] Biroli G and Kotliar G 2002 *Phys. Rev. B* **65** 155112
[30] Maier T, Jarrell M, Pruschke T and Hettler M H 2005 *Rev. Mod. Phys.* **77** 1027
[31] Park H, Haule K and Kotliar G 2008 *Phys. Rev. Lett.* **101** 186403
[32] Parcollet O and Biroli G 2004 *Phys. Rev. Lett.* **92** 226402
[33] Rubtsov A N, Savkin V V and Lichtenstein A I 2005 *Phys. Rev. B* **72** 035122
[34] Tao H S, Chen Y H, Lin H F, Liu H D and Liu W M 2014 *Sci. Rep.* **4** 5367
[35] Metzner W and Vollhardt D 1989 *Phys. Rev. Lett.* **62** 324
[36] Georges A, Kotliar G, Krauth W and Rozenberg M J 1996 *Rev. Mod. Phys.* **68** 13
[37] Müller-Hartmann E 1989 *Z. Phys. B* **74** 507
[38] Jarrell M and Gubernatis 1996 *Phys. Rep.* **269** 133
[39] Chen Y H, Hung H H, Su G X, Fiete G A and Ting C S 2015 *Phys. Rev. B* **91** 045122
[40] Rozenberg M J, Chitra R and Kotliar G 1999 *Phys. Rev. Lett.* **83** 3498